STRUCTURAL SCIENCE
CRYSTAL ENGINEERING
MATERIALS

ISSN 2052-5206

Topotactic desolvation and oriented intergrowth in an iron(II) pincer complex

Matthias Käfer,[a] Berthold Stöger[b]* and Karl Kirchner[a]

[a]Institute of Applied Synthetic Chemistry, TU Wien, Getreidemarkt 9, 1060 Vienna, Austria, and [b]X-Ray Center, TU Wien, Getreidemarkt 9, 1060 Vienna, Austria. *Correspondence e-mail: bstoeger@mail.tuwien.ac.at

Received 21 July 2026
Accepted 28 September 2026

Edited by K. Dziubek, University of Vienna, Austria

Keywords: pincer complex; solvate; oriented intergrowth; topotactic transition; polytypism.

CCDC references: 2591342; 2591343

Supporting information: this article has supporting information at journals.iucr.org/b

Crystals of an oriented intergrowth of the Fe^{II} pincer complex **1** [$P2_1/c$, $Z = 4$, a = 12.3065 (9) Å, b = 11.8079 (6) Å, c = 22.2640 (15) Å, β = 101.097 (6)°, V = 3174.8 (4) Å^3] and its hemi-pentane solvate [$P2_1/c$, $Z = 4$, a = 14.6190 (4) Å, b = 11.7744 (2) Å, c = 21.8934 (7) Å, β = 113.556 (2)°, V = 3454.47 (17) Å^3] were analyzed using X-ray single-crystal diffraction. The structures of both phases were determined in a combined refinement against the same data set with reflection overlap information. The structures contain geometrically equivalent (up to moderate distortion) layers of Fe^{iPr}PCP(CO)(COPr)(NC^{t}Bu) (**1**) extending parallel to (100) and can therefore be described as being part of a polytype family, if the solvent molecule is considered as an impurity between the layers. On standing, crystals lose pentane, ultimately transforming into the non-solvate in a topotactic reaction.

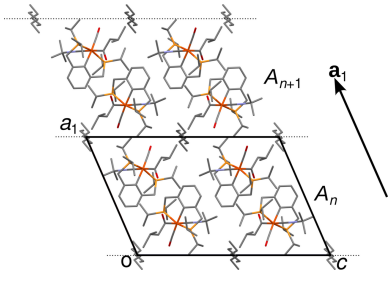
1. Introduction

Since the first half of the 20th century, single-crystal diffraction is the preferred method of structural analysis owing to its unparalleled reliability and robustness. The method is based on the *independent* evaluation of individual reflection intensities (Bruce *et al.*, 2014).

However, not all compounds crystallize as perfect single crystals. For example, systematic twinning leads to partial or full overlap of reflections of twin mates with different orientation states (Grimmer & Nespolo, 2006). From a practical point of view, structure derivation from twins can be considered as solved. Fully or partially overlapping reflections are integrated to a single intensity value, which is then modeled as the weighted sum of two or more intensities.

A more challenging case arises when a crystalline edifice is built of *structurally different* domains. If the orientations are not random, a large number of reflection overlaps may preclude independent refinement against only the non-overlapping reflections. Such is often the case for *allotwins*, the oriented intergrowth of distinct polytypes. Filonenko *et al.* (2013) refined two domains of an allotwin of an Ru PNP-pincer (coordinating in meridional fashion via P, N and P) complex in two steps: first by refining against non-overlapping reflections and then separating the overlapping reflections according to the expected ratios derived from these models. The *JANA* software suite (Petříček *et al.*, 2023) can refine two structures simultaneously against a reflection file with overlap information. We have applied this approach for example to the allotwin of an Re PNP-pincer complex (Glatz *et al.*, 2017).

A more obscure reason for such systematic intergrowths is an oriented intergrowth of a non-solvate and a solvate as our group has reported for an Fe PNN-pincer complex (Stöger *et al.*, 2015) and its dichloromethane (DCM) solvate.

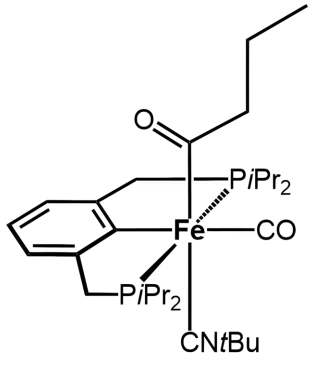


OPEN ACCESS
Published under a CC BY 4.0 licence

Table 1
Crystal data of both domains.

	1·0.5-pentane	**1**
Chemical formula	$C_{30}H_{51}FeNO_2P_2$·-(C_5H_{12})	$C_{30}H_{51}FeNO_2P_2$
M_r	611.6	575.5
μ (mm^{-1})	4.57	4.95
Crystal system, space group	Monoclinic, $P2_1/c$	Monoclinic, $P2_1/c$
a, b, c (Å)	14.6190 (4), 11.7744 (2), 21.8934 (7)	12.3065 (9), 11.8079 (6), 22.2640 (15)
β (°)	113.556 (2)	101.097 (6)
V (Å^3)	3454.47 (17)	3174.8 (4)
Z	4	4
$\Delta\rho_{max}$, $\Delta\rho_{min}$ (e Å^{-3})	0.37, −0.36	0.89, −0.39
Volume fraction	0.7729 (12)	0.2271 (12)

Herein we report another Fe PCP-pincer complex, Fe$^{i\mathrm{Pr}}$PCP(CO)(COPr)(NC^{t}Bu) (**1**, Scheme 1, IUPAC name: [(Butanoyl)(2,6-bis((bis(1-methylethyl)phosphino-κP)-methyl)phenyl-κC)(carbonyl)(*t*-butylisocyanide)iron(II)]), which forms oriented intergrowths of the hemi-pentane solvate **1**·0.5-pentane (major domain) and neat **1** (minor domain). Refinement proved challenging, owing to disorder and mediocre diffraction quality.



1

2. Experimental

2.1. Synthesis and crystal growth

The synthesis of **1** is given in Käfer *et al.* (2026). Crystals were obtained by cooling a concentrated solution in *n*-pentane stored under Ar atmosphere in a glass vial to 243 K.

2.2. Single-crystal diffraction and data processing

Intensity data of crystals attached to Kapton micro mounts with perfluorinated polyether were collected using Cu $K\alpha$ radiation on a Stoe STADIVARI diffractometer system equipped with a DECTRIS EIGER CdTe hybrid photon counting detector in a dry stream of nitrogen at 200 K. Data were processed using the *X-Area* software suite (Stoe & Cie, 2021) and a correction for absorption effects applied using the multi-scan approach implemented in *LANA* (Stoe & Cie, 2021).

The structures were solved with *SHELXT* (Sheldrick, 2015) and refined against F^2 with *Jana* (Petříček *et al.*, 2023). In the final refinement cycles, reflections with $|F_{obs} - F_{calc}| > 10\sigma(F_{obs})$ were omitted.

Table 2
Data collection and refinement.

The total number of reflections were derived from the original HKLF5 file, the number of independent (and observed) reflections from the reflection list output by *JANA*. No R_{int} value is given as it is ill-defined owing to different merging of overlapping and non-overlapping reflections.

Radiation type	Cu $K\alpha$
Crystal size (mm)	0.18 × 0.13 × 0.04
Diffractometer	Stoe STADIVARI
Temperature (K)	200
Absorption correction	Multi-scan (*LANA*)
T_{min}, T_{max}	0.249, 0.337
No. of measured, independent and observed [$I > 3\sigma(I)$] reflections	
total	47703, 22336, 13918
domain 1	14333, 4015, 3120
domain 2	17989, 3255, 1506
overlaps	15381, 15066, 9292
$(\sin\theta/\lambda)_{max}$ (Å^{-1})	0.605
Refinement $R[F^2 > 2\sigma(F^2)]$, $wR(F^2)$, S	0.061, 0.156, 1.5
No. of reflections	22336
No. of parameters	658
No. of restraints	14
H-atom treatment	H-atom parameters constrained

Intensity data of the **1**·0.5-pentane/**1** intergrowth was processed into a reflection file with overlap information ('HKLF5' format). The intensities of non-overlapping reflections of both domains were separated and the structures solved and refined separately. The models were then combined into a single refinement against the HKLF5 dataset. Refinements converged extremely slowly and distance restraints as well as constraints on the atomic displacement parameters of disordered groups had to be applied.

A non-reduced setting was chosen for **1** for a simpler description: in the chosen setting it shares the **a** and **b** basis vectors with **1**·0.5-pentane.

Data collection and refinement details are compiled in Tables 1 and 2.

3. Results and discussion

3.1. Crystals under investigation

We tested multiple crystal fragments with short X-ray diffraction experiments. All tested crystals featured splitting of reflections, which we erroneously attributed to classical twinning. Owing to mediocre diffraction quality (pronounced mosaicity) of the first screened crystals, we suspected a phase transition. Accordingly, we increased the measurement temperature to 200 K from our standard temperature of 100 K. Data of the most promising crystal was then collected in 6.6 h with with 0.5° ω-scans and 50.0 mm detector distance aiming for fivefold redundancy up to 2θ = 140° and 10 s exposure per frame. In total 2366 frames were collected.

After completing the data collection, the standard routine for twin indexing failed. We therefore separated the reflections manually, resulting in two domains with different metrics, which turned out to be **1**·0.5-pentane (*ca* 77% volume frac-

tion) and **1** (*ca* 23%). The data was processed as described in Section 2.2. The mask size was chosen optically accounting for the rather pronounced mosaicity.

Since the measurement was not optimized for such an unusual case, we tried to collect improved data of a second crystal at 100 K. However, the crystals, which were stored for *ca* 24 h on a microscopy slide under perfluorinated polyether, had lost all pentane and consisted only of non-solvate **1**. Diffraction quality was likewise mediocre, which is common for crystals generated by solid-to-solid phase transitions. The structural data derived from such a desolvated crystal are presented in Käfer *et al.* (2026) and correspond well to the structure of the minor **1** domain of the first crystal. Note that intensity data of the desolvated crystal were collected at 100 K, which invalidated our assumption of a phase transition.

We therefore presume that **1** crystallizes as the hemi-pentane solvate, which slowly loses solvent in a topotactic reaction, leading first to an **1**·0.5-pentane/**1** intergrowth and then ultimately to neat **1**.

3.2. Crystal structures

The structures of **1**·0.5-pentane and **1** (Fig. 1) are closely related and both possess isomorphic $P2_1/c$ symmetry with similar *b* and *c* cell parameters. In contrast, *a* and β differ significantly. The unit cell volume in **1**·0.5-pentane is larger by 279.7 Å^3 to accommodate for the additional two pentane molecules per unit cell. In both cases, **1** is located on the general position.

As suggested by the lattice parameters, **1**·0.5-pentane and **1** can be considered as being polytypes (Aksenov *et al.*, 2023) built of layers extending parallel to the (100) plane. Layer interfaces are indicated in Fig. 1 by dotted lines and individual layers are shown in Fig. 2. The layers possess $p_a12_1/c1$ symmetry, where the *ad hoc* subscript of the Bravais letter gives the direction without translation symmetry. The *International Tables for Crystallography*, Vol. E (Kopsky & Litvin, 2006) only define layer group symbols for groups whose translation lattice is spanned by (**a**, **b**).

In both cases, adjacent layers are related by translation along the respective **a** vector, which we will call $\mathbf{a}_1$ (**1**·0.5-

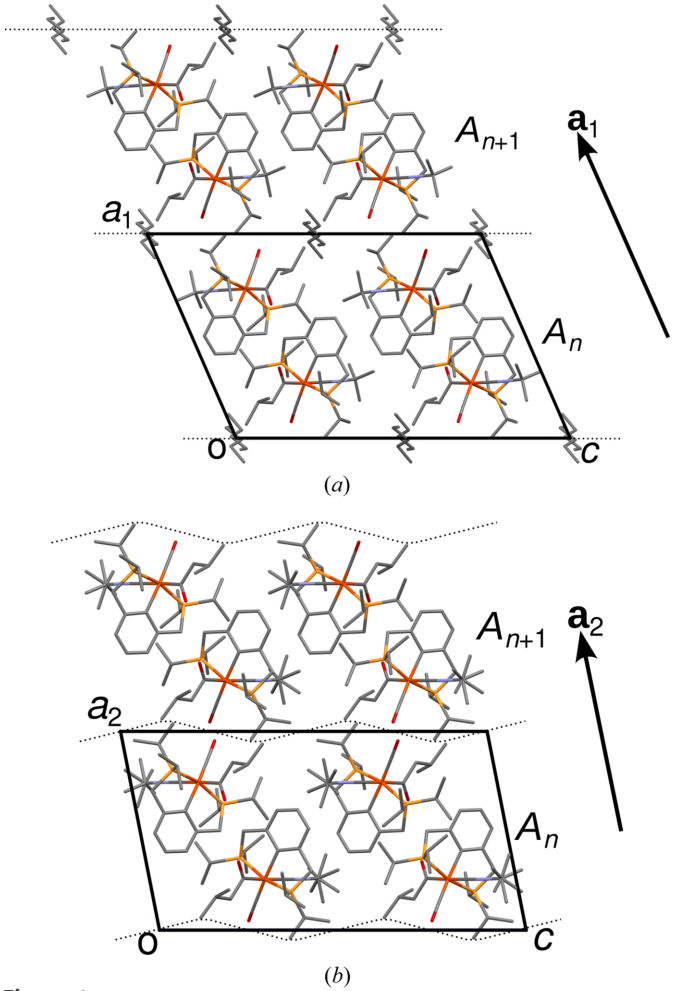


Figure 1
Capped stick representation of the structures of (*a*) **1**·0.5-pentane and (*b*) **1** viewed along [010]. Color codes: Fe orange, P yellow, O red, N blue and C gray. H atoms are omitted for clarity. Dotted lines mark the interfaces between polytype layers.

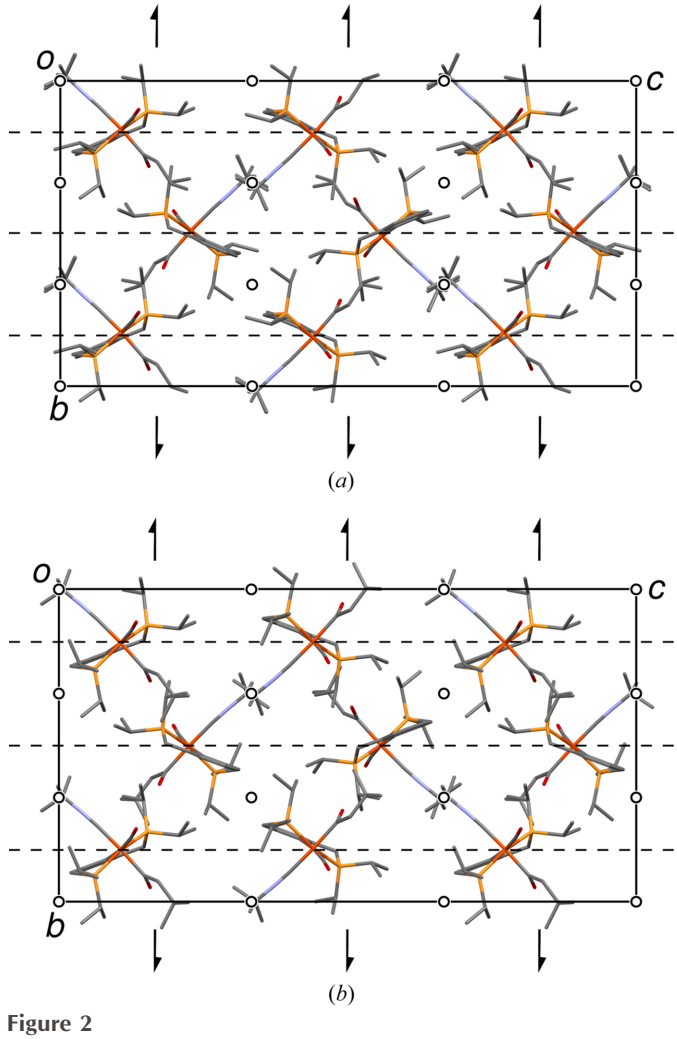


Figure 2
Layers of **1** molecules in (*a*) **1**·0.5-pentane and (*b*) **1** projected on the layer plane (100). Symmetry elements of the layer are indicated using the standard graphical symbols.

pentane) and $\mathbf{a}_2$ (**1**), both normal to **b**. The set of operations relating adjacent layers are obtained by forming the left coset of the layer group $p_a2_1/c1$ with the translation $\mathbf{a}_1$ or $\mathbf{a}_2$ and consists of translations, inversions, screw rotations and glide reflections. In **1**·0.5-pentane, pentane molecules are disordered about inversions relating adjacent layers.

Application of successive $\mathbf{a}_1$ or $\mathbf{a}_2$ translations can in principle lead to crystals with arbitrary pentane contents in the range $[0, \frac{1}{2}]$ per **1** molecule (only $\mathbf{a}_1$: $\frac{1}{2}$, only $\mathbf{a}_2$: 0). The crystal under investigation can be considered as such a stacking arrangement where macroscopic domains of successive $\mathbf{a}_1$ or $\mathbf{a}_2$ alternate. It therefore is an allotwin.

Observe that here we apply a loose definition of polytypism and consider the additional solvent molecule as a 'small amount of impurity' (Guinier *et al.*, 1984) at the layer interface. Both structures belong to the same polytype family only if the pentane molecules are ignored.

Since translation by $\mathbf{a}_1$ and $\mathbf{a}_2$ result in two geometrically different layer contacts, the polytypism is classified as being of the non-OD kind (Dornberger-Schiff & Grell-Niemann, 1961). See Kader *et al.* (2017) or Schöbinger & Stöger (2024) for more examples and details on non-OD polytypes.

3.3. Desymmetrization

Since layers in different members of a polytype family are located in different environments, one can expect desymmetrization (Ďurovič, 1979), which means that the layers are not perfectly (geometrically) equivalent. In non-OD polytypes, where the layer contacts differ significantly, one would expect particularly pronounced desymmetrization.

This is in fact the case in the crystal under investigation, where, as noted above, we consider the incorporation of the solvent molecules at the layer interfaces as a kind of 'desymmetrization'. Notably, the layer cell parameters *c* differ distinctly (by *ca* 1.7%, see Table 2).

Moreover, the individual molecules adopt conformational changes as shown in Fig. 3. The C12–C14 iso-propyl group (Fig. 3, right), which contacts to the pentane molecule in **1**·0.5-pentane, features different orientations in both polytypes. The *tert*-butyl isocyanide ligand (C22–C25, Fig. 3, top) is ordered in **1**·0.5-pentane (though with enlarged ADPs) but disordered about two position in the non-solvate **1**. Finally, the propionyl ligand (Fig. 3, bottom) is disordered in both structures, but with distinct occupancy ratios [55.7:44.3 (8) in **1**·0.5-pentane versus 65.8:34:2 (9) in **1**].

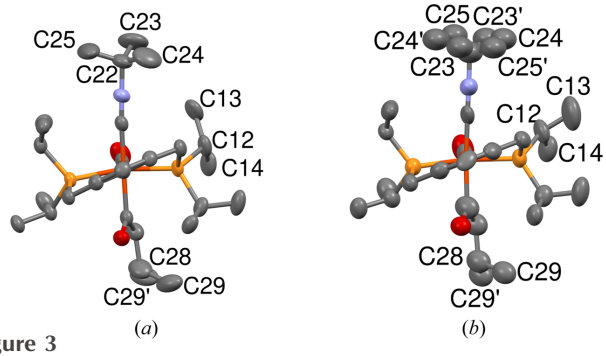


Figure 3
Complexes in the structures of (*a*) **1**·0.5-pentane and (*b*) **1**. Atoms are represented by displacement ellipsoids drawn at the 50% probability level with color codes as in Fig. 1. H atoms are omitted for clarity.

3.4. Diffraction pattern

Fig. 4 shows the $k = 2$ plane of reciprocal space of the **1**·0.5-pentane/**1** intergrowth. Ignoring desymmetrization of the metric parameters (assuming equal *b* and *c*), the direct bases of both components are ($\mathbf{a}_1$, **b**, **c**) and ($\mathbf{a}_2$, **b**, **c**), respectively (as before, the subscript 1 stands for the major **1**·0.5-pentane domain and 2 for the minor **1** domain). Since **b** is normal to $\mathbf{a}_1$, $\mathbf{a}_2$ and **c**, the reciprocal bases of both domains share the same **b*** vector, which is parallel to **b** and of inverse length. Thus, the reciprocal bases are $(\mathbf{a}_1^*, \mathbf{b}^*, \mathbf{c}_1^*)^T$ (**1**·0.5-pentane) and $(\mathbf{a}_2^*, \mathbf{b}^*, \mathbf{c}_2^*)^T$ (**1**), respectively. The superscript *T* indicates the transpose, as reciprocal bases are written in crystallography as columns.

$\mathbf{a}_1^*$ and $\mathbf{a}_2^*$ are parallel (normal to the layer planes) and of different length, namely the inverse of the distance between two adjacent layers: $1/(a_1 \sin\beta_1)$ respectively $1/(a_2 \sin\beta_2)$. Let $\mathbf{c}_0^*$ be the vector parallel to **c** with length $1/c$ and $\mathbf{a}_0^*$ the vector parallel to **a** with length $1/c$. Then $\mathbf{c}_1^* = \mathbf{c}_0^* - (\cot\beta_1)\mathbf{a}_0^*$ and $\mathbf{c}_2^* = \mathbf{c}_0^* - (\cot\beta_2)\mathbf{a}_0^*$.

It follows that for fixed $k_1 = k_2$ and $l_1 = l_2$, reflections of both domains are located on the same line parallel to $\mathbf{a}_0^*$ (see vertical white line in Fig. 4). For fixed $k_1 = k_2$ and $h_1 = h_2$

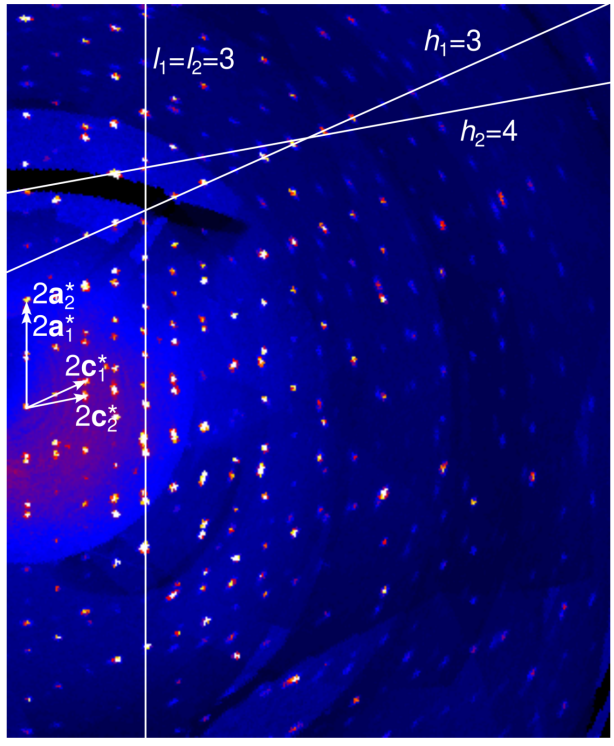


Figure 4
$k = 2$ section of reciprocal space of the crystal under investigation reconstructed from frame data. The $h_1 = 3$ line (of **1**·0.5-pentane), the $h_2 = 4$ line (of **1**) and the $l_1 = l_2 = 3$ line (both domains) are indicated by white lines.

reflections are located on distinct lines whose angle to $\mathbf{a}_0^*$ is the complement of β_1 and β_2, respectively (inclined lines in Fig. 4).

However, owing to desymmetrization, the layer cell parameters (b and c) in both domains are not precisely identical (see previous sections), which can be seen be reflections being slightly off the vertical line in Fig. 4), an effect which increases with higher $|l|$.

At higher diffraction angles, reflections show pronounced mosaicity, which can be rationalized by strain owing to lattice mismatch of the layers in domains 1 and 2 (notably $c_1 \neq c_2$) and crystal imperfections due to loss of solvent.

Absence of prominent diffuse scattering shows that the physical domains of both structures are macroscopic.

Overall, due to reciprocal lattices without a simple rational relationship and ill-defined reflection shapes, the best option to integrate intensities is a concurrent integration of both domains with overlap determination based on experimental peak profiles and orientation matrices (in contrast to using a common superlattice or using separate integrations and heuristics to determine reflection overlap).

3.5. Comparison with a previously published intergrowth

As mentioned in the introduction, we already discussed a similar intergrowth of the Fe PNN-pincer complex **2** and its mono-DCM solvate (Stöger *et al.*, 2015). There are a few fundamental differences to note though. Firstly, in **2**·DCM, the DCM molecules are arranged in distinct layers located between the Fe(PNN-^{i}Pr)Br$_2$ layers. Thus, the oriented **2**·DCM/**2** integrowths are classified as *merotypes* (Ferraris *et al.*, 2008) instead of polytypes (*meros* meaning partial in the sense that the structures share a part of the layers, but are different in others). Since the DCM layers possess a different symmetry than the layer contacts of the non-solvate, both domains possess different space group types.

The genesis of the intergrowths is different: whereas **1**·0.5-pentane/**1** intergrowths are most likely due to gradual loss of solvent, **2** • DCM/**2** crystals grow as-is with the content of the DCM solvate depending on the concentration of DCM in the solvent mixture. Therefore, the crystals of the latter were of significantly improved quality.

Finally, the desymmetrization is much less pronounced, with the **2** layers in the solvate and non-solvate deviating only marginally in their atomic positions, without any changes in conformation or disorder.

4. Conclusion

Out of necessity, in powder diffraction it is common practice to refine distinct structures against the same data set. In single-crystal diffraction, such refinements are very rare. Thus, besides featuring an interesting solid-to-solid phase transition, the crystal under investigation serves as a test case for such combined refinements.

We found that while possible, these refinements are still tricky. Partly for intrinsic reasons, such as correlation of parameters, but also because the refinement software stack is neither optimized nor tested for such a rare use-case. Many tools experimental crystallographers nowadays take as granted do not support multi-structure refinements. In particular, the CIF (Crystallographic Information File) format can only represent one structure per data block. Likewise, the crucial *CheckCIF* tool, which structural scientists heavily rely on, can only check one structure at a time and thus misinterprets diffraction data. This means that, like in the case of incommensurately modulated structures, one must exercise additional care.

Different thermal expansion coefficients might lead to better separation of diffraction spots on cooling. On the flip side, it may cause increased mosaicity owing to strain. Thus, multi-temperature experiments might be fruitful.

Finally, we note that while the crystal structure determination of small pincer complexes may appear mundane and routine, it is a treasure trove of complex crystallization behavior, of which the title compound is one further example.

Acknowledgements

The authors acknowledge Open Access funding provided by Technische Universitat Wien.

References

Aksenov, S. M., Charkin, D. O., Banaru, A. M., Banaru, D. A., Volkov, S. N., Deineko, D. V., Kuznetsov, A. N., Rastsvetaeva, R. K., Chukanov, N. V., Shkurskii, B. B. & Yamnova, N. A. (2023). *J. Struct. Chem.* **64**, 1797–2028.

Bruce, D. W., O'Hare, D. & Walton, R. I. (2014). Editors. *Structure from Diffraction Methods*. Hoboken: John Wiley & Sons.

Dornberger-Schiff, K. & Grell-Niemann, H. (1961). *Acta Cryst.* **14**, 167–177.

Ďurovič, S. (1979). *Cryst. Res. Technol.* **14**, 1047–1053.

Ferraris, G., Makovicky, E. & Merlino, S. (2008). *Crystallography of Modular Materials*, Vol. 15 of *IUCr Monographs on Crystallography*. Oxford: Oxford University Press.

Filonenko, G. A., Conley, M. P., Copéret, C., Lutz, M., Hensen, E. J. M. & Pidko, E. A. (2013). *ACS Catal.* **3**, 2522–2526.

Glatz, M., Stöger, B. & Kirchner, K. (2017). *Acta Cryst.* B**73**, 941–949.

Grimmer, H. & Nespolo, M. (2006). *Z. Kristallogr.* **221**, 28–50.

Guinier, A., Bokij, G. B., Boll-Dornberger, K., Cowley, J. M., Ďurovič, S., Jagodzinski, H., Krishna, P., de Wolff, P. M., Zvyagin, B. B., Cox, D. E., Goodman, P., Hahn, Th., Kuchitsu, K. & Abrahams, S. C. (1984). *Acta Cryst.* A**40**, 399–404.

Kader, T., Kautny, P., Stöger, B. & Fröhlich, J. (2017). *Z. Kristallogr.* **232**, 375–384.

Käfer, M., Gstöttner, S., Stöger, B., Dupé, A., Veiros, L. & Kirchner, K. (2026). *Organometallics* **45**, 2177–2184.

Kopsky, V. & Litvin, D. B. (2006). Editors. *International Tables For Crystallography*, Vol. E, *Subperiodic Groups*. Chester: IUCr.

Petříček, V., Plášil, L. P. J. & Dušek, M. (2023). *Z. Kristallogr.* **238**, 271–282.

Schöbinger, M. & Stöger, B. (2024). *Z. Kristallogr.* **239**, 331–338.

Sheldrick, G. M. (2015). *Acta Cryst.* A**71**, 3–8.

Stoe & Cie (2021). *X-AREA* 1.31.175.0, *LANA* 2.6.2.0. Stoe & Cie GmbH, Darmstadt, Germany.

Stöger, B., Holzhacker, H. & Kirchner, K. (2015). *Z. Kristallogr.* **230**, 621–628.